ARTICLE NO. 79-0143R

Scale Effects on Fluctuating Pressures in Spike-Induced Flow Separation

J. Peter Reding,*Rolf A. Guenther,† and Dennis M. Jecmen†
Lockheed Missiles & Space Co., Inc., Sunnyvale, Calif.

Data for 40% and 100% wind-tunnel models are compared with flight results. The separated region was found to increase in size with increasing Reynolds number even though the Reynolds number at reattachment was always turbulent. Futhermore, critical Reynolds number effects in the flow recirculation region caused the most severe fluctuating pressure on the spike to shift to the leeward side. Evidence of the excitation of a fundamental breathing mode of the spike-induced flow separation was observed on a second flight.

Nomenclature

A = forebody axial force; coefficient: $C_A = A/qS$
a = speed of sound
ΔC_{A0} = axial force coefficient increment due to Reynolds number variation
C_p = pressure coefficient = $(p - p_\infty)/q$
$C_{P(\text{rms})}$ = root-mean-square fluctuating pressure coefficient = $\Delta p_{(\text{rms})}/q$
D = drag; coefficient: $C_D = D/qS$
d = reference diameter
d_s = spike base diameter
f = frequency, Hz
L = spike length
M = Mach number
p = local pressure
p_∞ = freestream static pressure
PSD = power spectral density
$p(t)$ = time varying pressure
$\Delta p_{(\text{rms})}$ = fluctuating pressure = $\left[\frac{1}{T}\int_0^T [p(t)]^2 dt - p^2\right]^{1/2}$
q = freestream dynamic pressure = $\rho U^2/2$
r = spherical nose radius
R_L = freestream Reynolds number based on spike length = $\rho UL/\mu$
R_r = recirculatory Reynolds number based on spike base diameter = $\rho_r U_r d_s/\mu_r$
S = reference area = $\pi d^2/4$
s = model scale factor = d(model)/d(full scale)
U = freestream velocity
x = axial coordinate, origin at nose fairing tip
α = angle of attack
δ = viscous flow height
ϕ = roll orientation (0 = leeward)
ρ = freestream density

Subscripts

r = condition in recirculation region at spike base
∞ = freestream flow
1,2 = different Reynolds number values

Presented as Paper 79-0143 at the 17th Aerospace Sciences Meeting, New Orleans, La., Jan. 15-17, 1979; submitted Feb. 8, 1979; revision received July 30, 1979.

Index categories: LV/M Aerodynamics; Jets, Wakes and Viscid-Inviscid Flow Interactions; Nonsteady Aerodynamics.

*Staff Engineer. Associate Fellow AIAA.
†Research Specialist.

Introduction

THE Trident I missile is equipped with an extendible nose spike or "aerospike" that is deployed immediately after launch. The aerospike substantially reduces missile forebody drag by creating a low dynamic pressure region of separated flow over the high volume nose fairing (Fig. 1).[1,2] The telescoping design of the aerospike was thought to be particularly vulnerable to the severe fluctuating pressure environment that exists in regions of flow separation. Thus, extensive wind tunnel tests were conducted to define the fluctuating pressure environment of the aerospike/nose fairing combination.[1] The wind tunnel results showed that the lateral load on the aerospike due to the fluctuating pressures was two orders of magnitude more severe than the static aerodynamic load.[2] Thus, the fluctuating pressures constitute the critical lateral aerodynamic load on the aerospike. The drag of the spike disk is the critical axial load on the aerospike. It was, therefore, essential that the technique used to scale the wind tunnel fluctuating pressure data to full scale flight conditions be valid.

In order to verify the scaling technique as much as possible before flight, a 100% aerospike-nose cap model was tested at transonic speeds where the most severe fluctuating pressure environment occurs on the aerospike. These tests were run at full scale dynamic pressure; thus, duplicating flight Reynolds numbers. Unfortunately the 100% model could not be tested at supersonic speeds due to wind tunnel blockage considerations. Flight data, of course, furnished the final check of scaling methods. Results of both wind tunnel tests and flight are compared herein.

Configurations Tested

The 40% wind tunnel model was made of heavy-gage stainless steel. The configuration had a simple cylindrical aerospike and simulated the forward portion of an earlier nose fairing configuration (Fig. 2a). The entire aerospike and nose fairing well aft of flow reattachment were equipped with static and fluctuating pressure instrumentation. The model was tested in the AEDC 16 ft Transonic Wind Tunnel and NASA Lewis Research Center 10×10 ft Supersonic Wind Tunnel.[1]

The 100% model was actually a full scale, flight hardware, aerospike, and nose cap (Fig. 2b). The entire nose fairing could not be tested because of wind tunnel blockage constraints. Only the nose cap and spike base were supplied with static and fluctuating pressure instrumentation. As previously stated, the model was tested in the 16 ft Transonic Wind Tunnel at conditions duplicating flight.

Because of limitations of telemetry channels and due to the telescoping nature of the aerospike, the fluctuating pressures were measured at only three locations on the nose fairing in

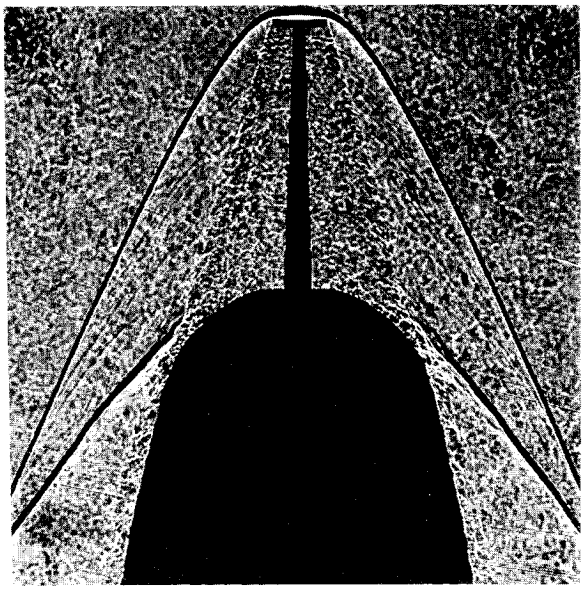

Fig. 1 Aerospace flowfield, $M=3.0$.

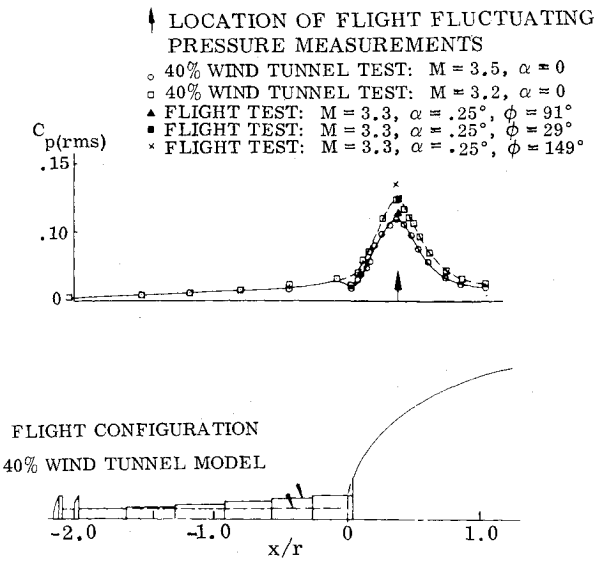

Fig. 3 Comparison of longitudinal fluctuating pressure distributions for $M=3.2$ and $M=3.5$.

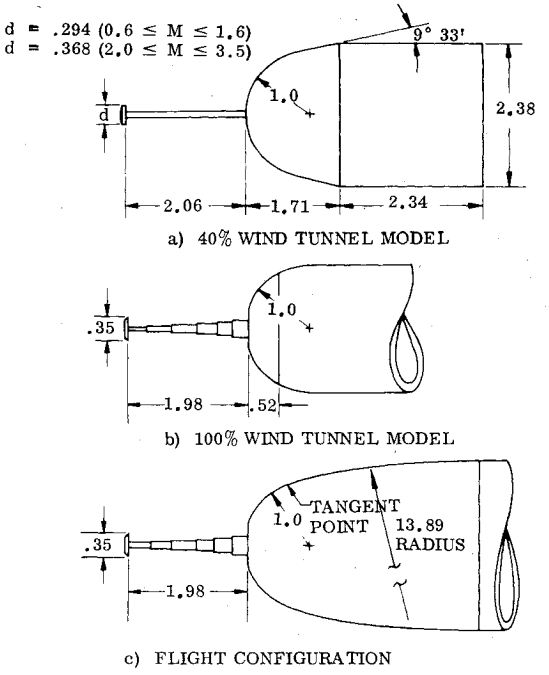

Fig. 2 Comparison of test configurations.

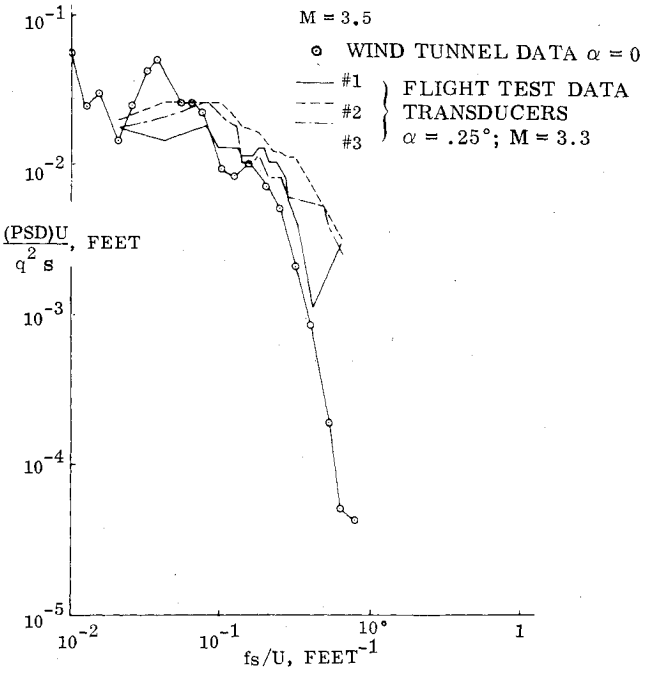

Fig. 4 Comparison of spectra at $M=3.5$, $x/r=0.37$.

flight. These were located 120 deg apart circumferentially and at $x/r=0.37$ aft of the nose tip; the location of flow reattachment on the 40% model at $M=3.0$. The flight vehicle nose fairing-aerospike configuration is compared with the wind tunnel model configurations in Fig. 2. The configuration differences do affect the data as will be shown later.

The 100% model duplicated the flight Reynolds number whereas the Reynolds number for the 40% model varied from ½ to ⅛ of the flight Reynolds number depending on the Mach number. For all models the Reynolds number based on spike length (R_L) was solidly turbulent. Even the 40% model produced $R_L \geq 4\times10^6$. Thus, the flow at reattachment was turbulent for all tests.

Data Analysis

The 40% wind tunnel data showed that the power spectra in the separated flow region would collapse into a few characteristic spectral types[1] if the data were nondimensionalized as suggested by Coe and Chyu.[3] That is, the power spectra values (PSD's) were multiplied by $U/q^2\delta$ and the frequency f by δ/U; where U and q are the freestream velocity and dynamic pressure, respectively, and δ is the local viscous flow (the flow separation) thickness. If the separated flow configuration is similar for both ground and flight test then the model scale factor s can be substituted for δ. Thus, if the normalized spectrum and the integral of that spectrum, $C_{p(\mathrm{rms})}$, are in agreement for wind tunnel and flight then the wind tunnel has supplied a valid simulation of flight.

The fluctuating pressure transducers on the flight vehicle were located at $x/r=0.37$ to measure the fluctuating pressure peak associated with flow reattachment at maximum dynamic pressure (at $M\approx3.0$). The good agreement between flight and 40% wind tunnel model data for both the overall fluctuating pressures and the semi-normalized spectra are shown in Figs. 3 and 4, respectively. This, of course, substantiates the validity of the scaling techniques.

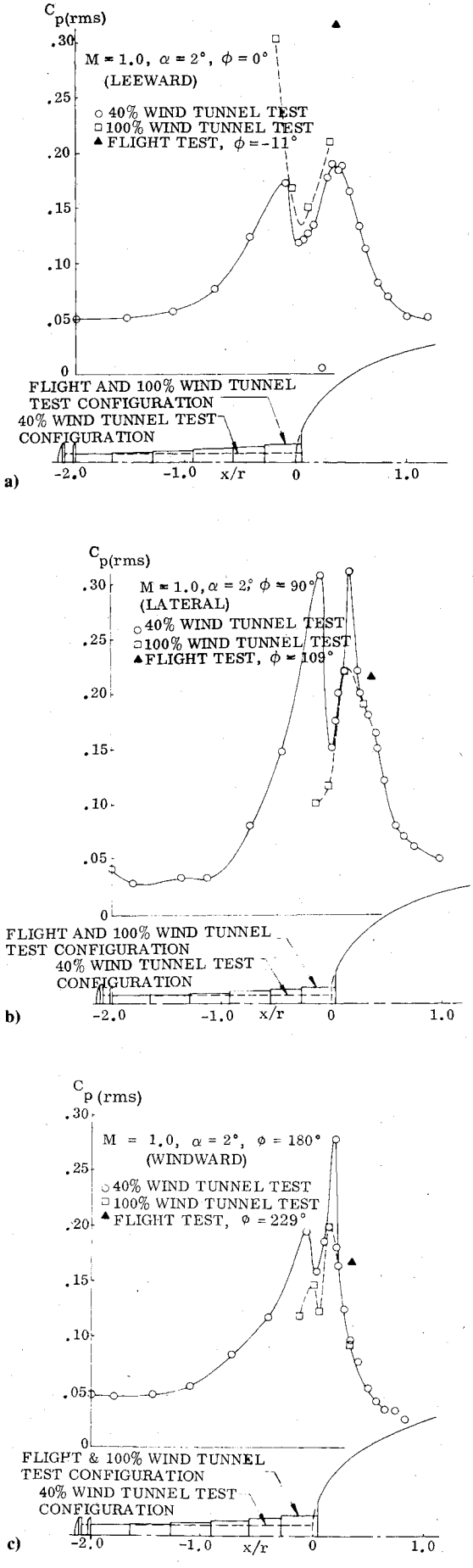

Fig. 5 Comparison of longitudinal fluctuating pressure distributions on a) the leeward meridian, b) the lateral meridian, and c) windward meridian for $M = 1.0$.

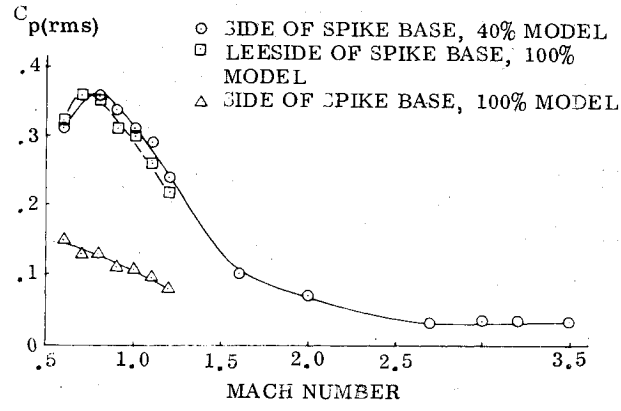

Fig. 6 Comparison of peak fluctuating pressures on the spike base at $\alpha =$ deg.

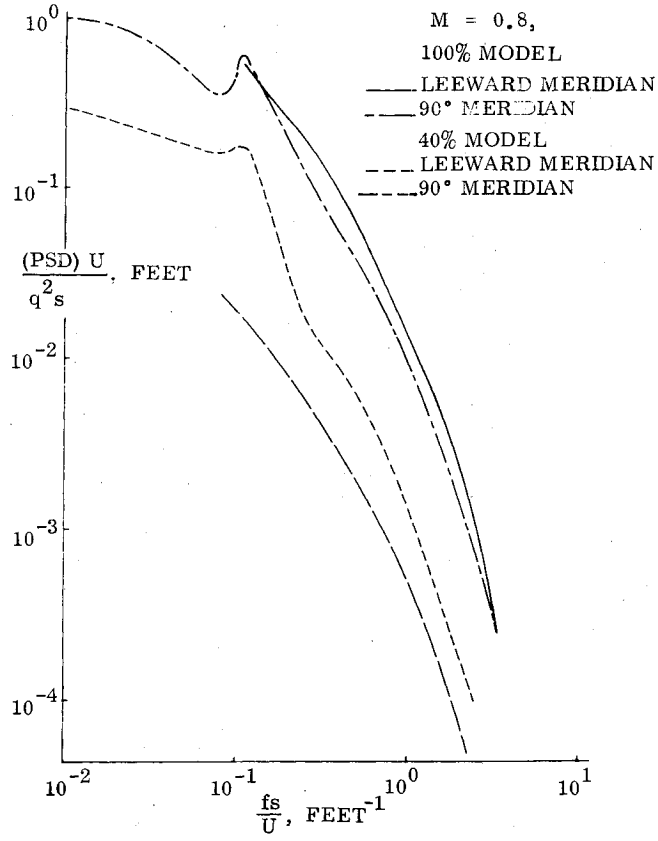

Fig. 7 Comparison of spectra on the spike base.

Reynolds Number Effects

At transonic speeds the fluctuating pressure peak occurs well forward of the flight transducers indicating that the separated region is smaller than it was at $M = 3.0$ (Fig. 5). Figure 5 also reveals a fundamental difference between the fluctuating pressure distributions for the 40% and 100% model tests. The flight data tend to support the 100% model data. The peak fluctuating pressure occurs on the leeside of the spike for the 100% model whereas it occurs on the lateral meridian of the 40% model (Figs. 5a and b). However, the flight data show a fluctuating pressure peak on the leeside of the nose fairing that appears to be associated with the environment at the spike base (Fig. 5a). Comparison of the overall fluctuating pressure $C_{p(rms)}$ values for the 40 and 100% models show that the high $C_{p(rms)}$ values measured at transonic speeds on the sides of the spike of the 40% model appear to have moved to the leeside of the spike on the 100% model (Fig. 6). Likewise, the semi-normalized spectra on the sides of

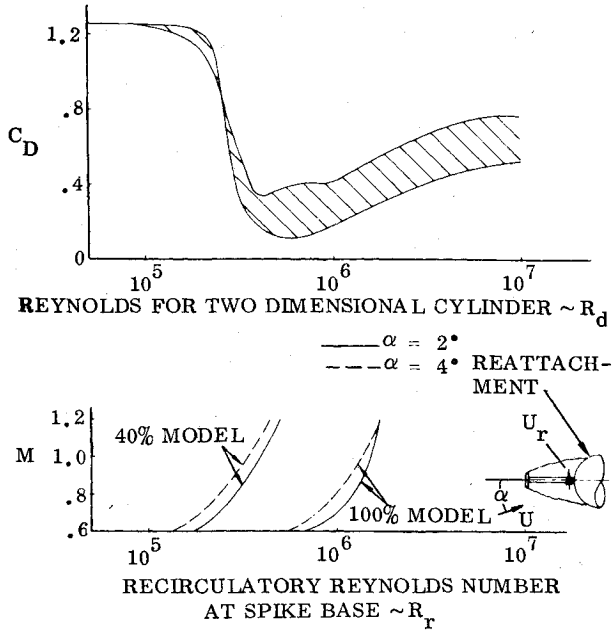

Fig. 8 Critical Reynolds number effects in the recirculation region.

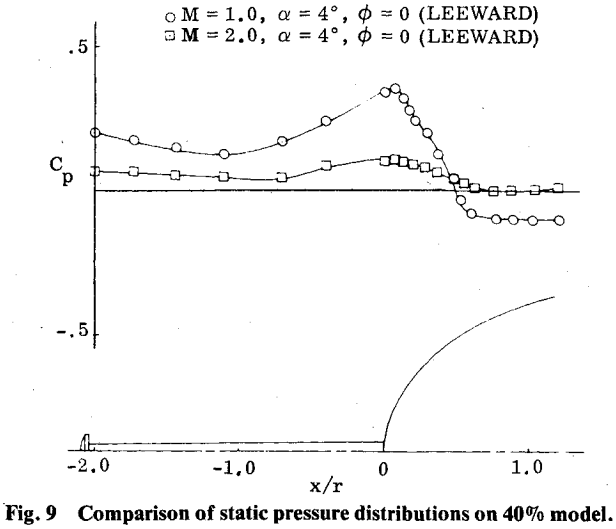

Fig. 9 Comparison of static pressure distributions on 40% model.

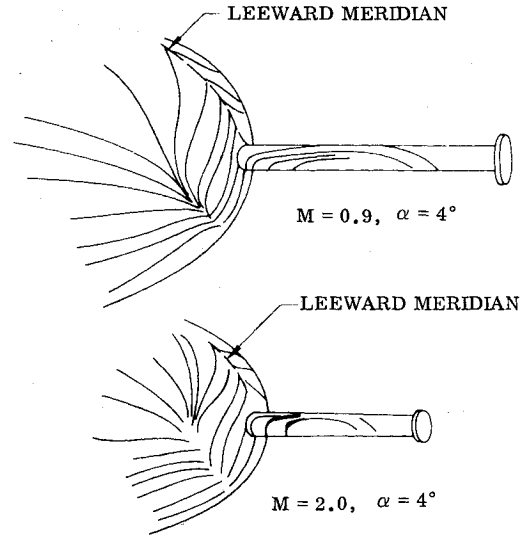

Fig. 10 Tracings from oil flow photographs.

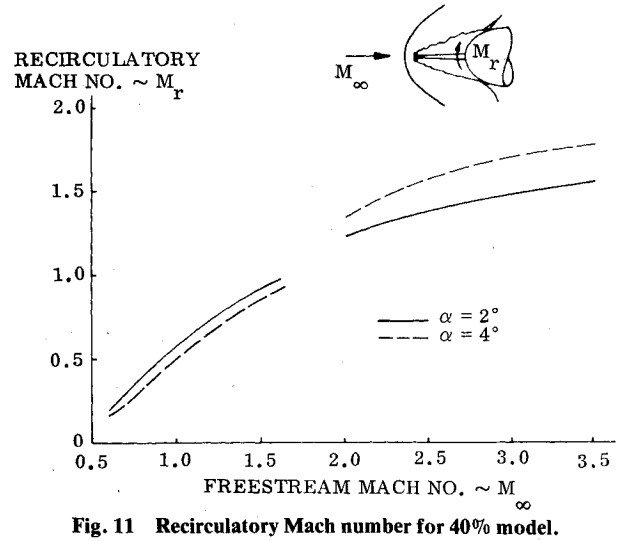

Fig. 11 Recirculatory Mach number for 40% model.

the spike of the 40% model are in good agreement with the spectra on the leeside of the spike of the 100% model (Fig. 7). This indicates that the same flow phenomenon is responsible for both. The present analysis will show that peak fluctuating pressure on the spike base is due to a secondary separation of the recirculatory flow and shifts to the leeside of the spike due to critical Reynolds number effets similar to those observed on cylinders normal to the flow.

One can define a crossflow Reynolds number in the recirculation region at the spike base by simply isentropically expanding the flow from the stagnation conditions at the windward reattachment point to the spike base. This recirculatory Reynolds number R_r is compared to the drag curve for a cylinder normal to the flow[4] (Fig. 8). The R_r values are subcritical for the 40% model and supercritical for the 100% model. At subcritical Reynolds number the flow separates near the lateral meridian of the cylinder whereas at supercritical Reynolds number the separation occurs 30-40 deg to the leeward of the lateral meridian.

It appears that the peak fluctuating pressures on the spike base could be associated with the secondary separation of the recirculating flow. Actually, the flow in the crossflow plane of the spike does not separate. Rather, at the point of incipient separation the upstream pressure gradient (Fig. 9) begins to dominate, turning the flow upstream along the spike (Fig. 10). The maximum fluctuating pressure corresponds to the point of maximum streamline curvature. This explains why the maximum fluctuating pressure occurs on the spike sides for the 40% model at transonic speeds. Further upstream along the spike, the flow is predominantly forward and the crossflow analogy no longer applies.

At supersonic speeds the Reynolds number is also subcritical but flow turning at the spike base occurs near the leeward meridian (Fig. 10). This is because the crossflow Mach number in the recirculation region is supersonic (Fig. 11) and at supersonic speeds separation occurs well aft of the lateral meridian on a cylinder.[5] Of course the crossflow Mach numbers calculated by expanding the flow from reattachment conditions to the spike base are ideal values as are the values of R_r. Viscous effects will tend to reduce both R_r and the crossflow Mach number; however, circumferential pressure distributions around the spike base show a typically subsonic, subcritical, distribution at $M=1.0$ relative to the $\alpha=0$ level and a supersonic distribution at $M=2.0$ indicating that the crossflow is indeed supersonic for $M\geq 2.0$ (Fig. 12). This is remarkable since the flow is not simply sweeping across the spike from windward to leeward but is also converging on the spike from the sides (Fig. 10). One would think the converging flow would significantly alter the location of the separation points relative to two-dimensional cylinder values.

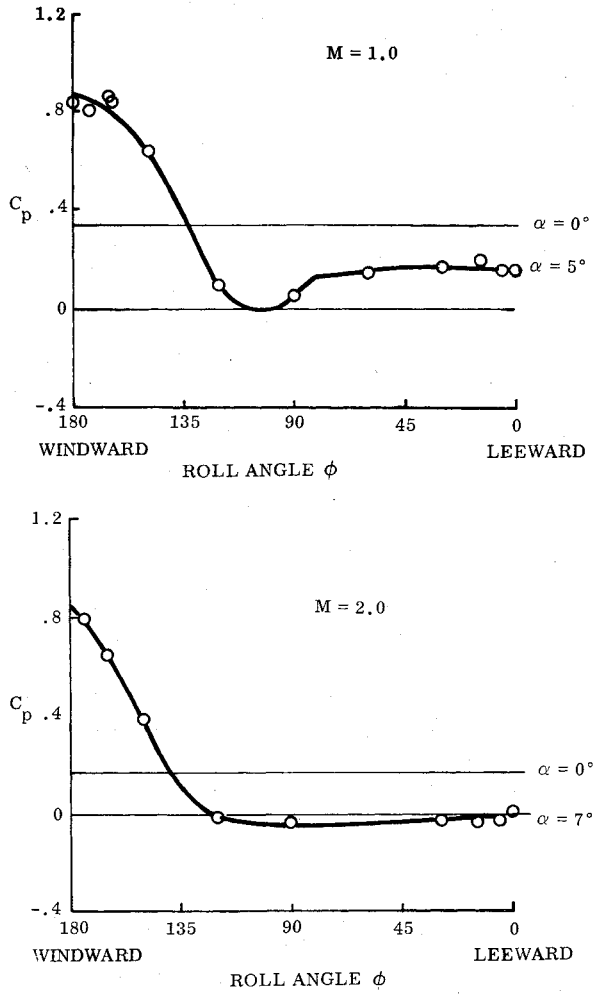

Fig. 12 Circumferential pressure distributions on spike base, 40% model.

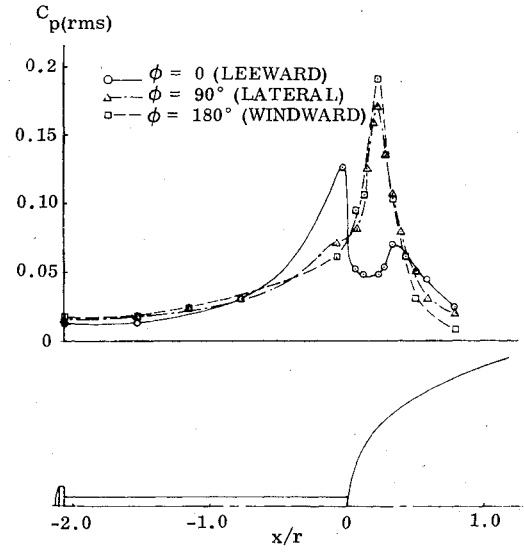

Fig. 13 Typical supersonic fluctuating pressure distribution on the 40% model, $M = 2.0$, $\alpha = 4$ deg.

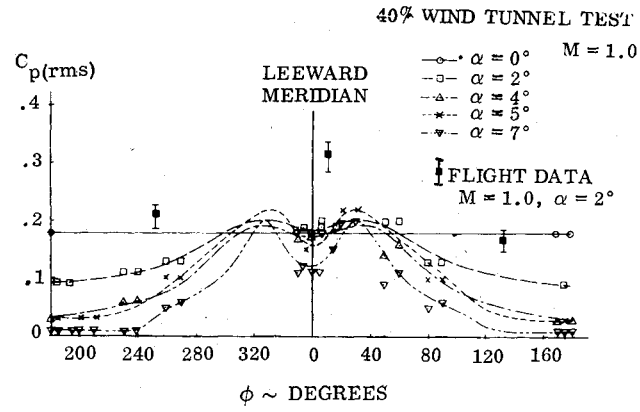

Fig. 14 Comparison of transonic fluctuating pressures at $x/r = 0.37$ aft of nose tip.

The peak fluctuating pressure occurs on the leeside of the spike at supersonic speed (Fig. 13), verifying the correlation between streamline curvature and peak fluctuating pressure. Thus, at supersonic speeds the fluctuating pressures on the spike base are in good agreement for both 40 and 100% wind tunnel models because the recirculatory flow is supersonic for both. The supersonic flow eliminates the sensitivity of the flow separation location to Reynolds number effects as well as moving separation to the leeside. The well known insensitivity of the crossflow drag of a cylinder at transonic-supersonic speeds,[6] is evidence of this Reynolds number freeze phenomenon.

The flight data indicate that the peak fluctuating pressure also occurs on the leeside of the spike at transonic speeds; which, of course, it should since flight and 100% wind tunnel model data are for identical Mach number-Reynolds number histories. Data from the 40% wind tunnel model show that the peak fluctuating pressure on the spike base is reflected in a similar peak on the nose fairing (Fig. 5b). This peak occurs on the leeward side in flight (compare Figs. 5a and 5b) thus, 100% model data and flight data are in agreement.

Even though the flight and 100% model data agree qualitatively, at transonic speeds the flight $C_{p(rms)}$ values are somewhat above the 100% model data (Figs. 5b and 5c). This could be a bonafide difference or it could be the result of errors in the computed flight angles of attack. The flight angle of attack is computed from atmospheric wind measurements taken before the flight. Subsequent wind changes at the time of flight could cause errors in angle of attack which could result in asymmetries of the flow reattachment geometry affecting the flight $C_{p(rms)}$ measurements. However, Fig. 14 shows that rather extreme variations in α could not cause the high values of $C_{p(rms)}$ observed in flight. Based on wind measurements before and after the flight α variations of only 1 or 2 deg can occur due to winds. Therefore, it appears that the $C_{p(rms)}$ differences are due to the configuration differences between the 100% model and the flight vehicle (compare Figs. 2b and 2c).

Typical static pressure data show that the pressures on the 100% model tend to be generally below the flight results. Although this difference is roughly within the error bands of the flight data, this trend pervades the data and is therefore believed to be real. It should be noted that the error bands on the flight data represent maximum expected α variations due to winds and may, therefore, be excessive. The expansion at the nose cap shoulder on the 100% model (Fig. 2b) is felt upstream at transonic speeds (subsonic speeds within the separated flow region). This decreases the level of both the static and fluctuating pressures over the nose cap and explains the lower static and fluctuating pressure levels on the 100% model relative to the flight data (Figs. 5 and 15).

The peak static pressure in flight tends to occur aft of the peak on the 40% model. This is also a pervasive trend within the error band of the flight data that is believed to be real. It is indicative of an increase in the size of the separated region in flight which results in a further separation-induced drag reduction. An estimate of this additional drag reduction was obtained by integrating the 40% model and flight static pressures and differencing the result. The resulting ΔC_{A0},

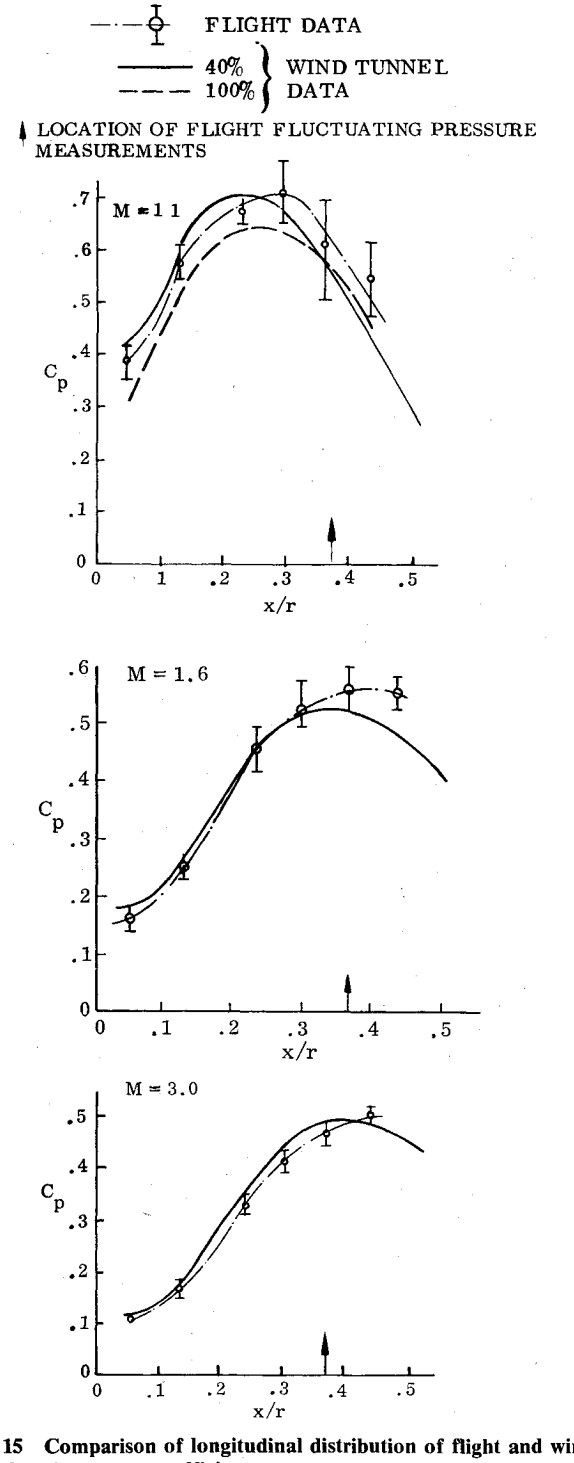

Fig. 15 Comparison of longitudinal distribution of flight and wind tunnel static pressure coefficients.

plotted as a function of R_L, is compared with similar incremental axial force measurements obtained in the NASA Marshall Space Flight Center High Reynolds Number Facility on a wind tunnel force balance[7] (Fig. 16). The wind tunnel data have been corrected for skin friction and base pressure effects and, thus, are indicative of forebody pressure drag effects only. This pressure drag reduction can only be the result of an expansion of the separated flow region. Both the 40% model-flight data comparison and the high Reynolds number wind tunnel data indicate that the size of the separated region grows with increasing, turbulent, Reynolds number; thus, full scale Reynolds numbers must be achieved in the wind tunnel in order to provide a valid simulation of flight characteristics.

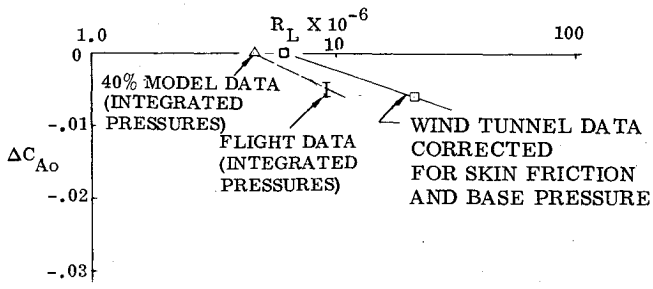

Fig. 16 Comparison of Reynolds number effects on spike-induced axial force increments, $M = 3.5$.

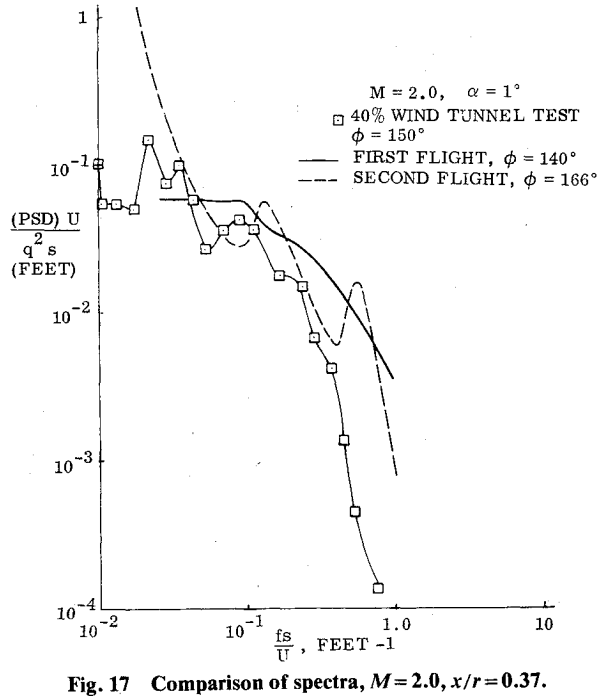

Fig. 17 Comparison of spectra, $M = 2.0$, $x/r = 0.37$.

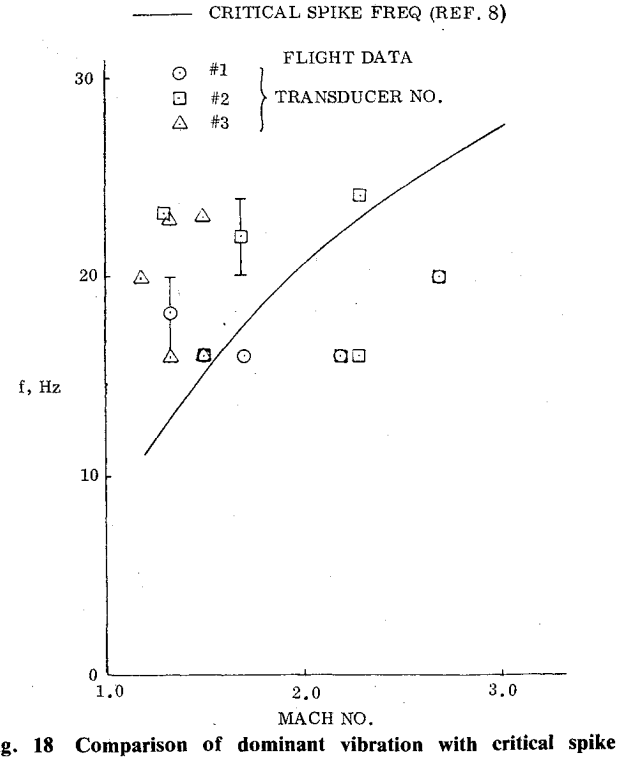

Fig. 18 Comparison of dominant vibration with critical spike frequency.

Flow Resonance Effects

Data from a second flight showed a strong low-frequency, periodic, pressure oscillation superimposed on the usual random pressure signal. This was observed on all three transducers and was strong enough in some cases to drive the signal to band edge. Except for the low frequency spike the spectra for the two flights were in essential agreement with one another and with 40% model results at $M \geq 2.0$ (Fig. 17). Within the accuracy of the data ($\approx \pm 5$ Hz), the frequency of the oscillation agrees well with Ericsson's critical breathing mode[8] for spike-induced flow separation (Fig. 18). Evidently, this is a fundamental breathing mode of spike-induced flow separation that can result in self-sustained oscillations for certain critical geometries and can also result in relatively innocuous oscillations for noncritical geometries. Fortunately our geometry is of the latter kind. It appears that a significant perturbation is required to excite the oscillation for noncritical geometries. In the case of the second flight a more severe angle-of-attack history is believed to be responsible for exciting this mode.

Conclusions

An analysis of scale effects on the fluctuating pressure environment in a region of spike-induced flow separation has shown two significant Reynolds number effects: 1) an increase in the size of the separated flow region with increasing turbulent Reynolds number, indicated by an aft movement of the peak static and fluctuating pressures; and 2) a critical Reynolds number effect in the recirculation region involving secondary flow separation on the spike shaft.

The sensitivity of the size of the separated region to Reynolds number points out the necessity of simulating full-scale Reynolds number in the wind tunnel since the static and fluctuating pressure distributions and the drag are all affected by the size of the separated region. Incidentally, this Reynolds number effect should be considered when trying to predict the drag of re-entry bodies with indented nose tips that also experience spike-induced flow separation. The critical recirculatory Reynolds number effects further emphasize the need to simulate full scale Reynolds number in ground test facilities.

The possibility of excitation of the fundamental breathing mode of the spike-induced separated flow region should be considered in the structural dynamics of any further aerospike designs.

References

[1] Guenther, R.A. and Reding, J.P., "Fluctuating Pressure Environment of a Drag Reduction Spike," *Journal of Spacecraft and Rockets*, Vol. 14, Dec. 1977, pp. 705-710.

[2] Reding, J.P., Guenther, R.A., and Richter, B.J., "Unsteady Aerodynamic Considerations in the Design of a Drag Reduction Spike," *Journal of Spacecraft and Rockets*, Vol. 14, Jan. 1977, pp. 54-60.

[3] Coe, C.F. and Chyu, W.J., "Pressure-Fluctuations Inputs and Response of Panels Underlying Attached and Separated Turbulent Boundary Layers," NASA TMX-62, 189, Sept. 1972.

[4] Jorgensen, L.H., "Prediction of Static Aerodynamic Characteristics for Slender Bodies Alone and with Lifting Surfaces to Very High Angles of Attack," NASA TR R-474, Sept. 1977.

[5] Gowen, F.E. and Perkins, E.W., "Drag of Circular Cylinders for a Wide Range of Reynolds Numbers and Mach Numbers," NACA TN 2960, June 1953.

[6] Jorgensen, L.H., "Prediction of Static Aerodynamic Characteristics for Bodies at Angles of Attack from 0° to 180°," NASA TN D-6996, Jan. 1973.

[7] French, N.J., "Investigation of Static Stability and Drag of the Trident I, C4 First Stage with Aerospike in the NASA Marshall Space Flight Center High Reynolds Number Wind Tunnel (E-81, C4A-7)," LMSC-D366909, Jan. 1974.

[8] Ericsson, L.E., "Flow Oscillations on Concave Conic Forebodies," AIAA Paper 77-1130, AIAA Atmospheric Flight Mechanics Conference, Hollywood, Fla., Aug. 1977.